To link to this article : DOI:10.1016/j.jsv.2013.08.046
URL : http://dx.doi.org/10.1016/j.jsv.2013.08.046

Accounting for convective effects in zero-Mach-number thermoacoustic models

E. Motheau [a,*], L. Selle [b,c], F. Nicoud [d]

[a] CERFACS - CFD Team, 42 av. Gaspard Coriolis, 31057 Toulouse, France
[b] Université de Toulouse, INPT, UPS, IMFT (Institut de Mécanique des Fluides de Toulouse), Allée Camille Soula, F-31400 Toulouse, France
[c] CNRS, IMFT, F-31400 Toulouse, France
[d] CNRS UMR 5149 - University Montpellier II, 34095 Montpellier, France

A B S T R A C T

This paper presents a methodology to account for some mean-flow effects on thermo-acoustic instabilities when using the zero-Mach-number assumption. It is shown that when a computational domain is represented under the $M=0$ assumption, a nonzero-Mach-number element can simply be taken into account by imposing a proper acoustic impedance at the boundaries so as to mimic the mean flow effects in the outer, not computed flow domain. A model that accounts for the coupling between acoustic and entropy waves is presented. It relies on a "delayed entropy coupled boundary condition" (DECBC) for the Helmholtz equation satisfied by the acoustic pressure. The model proves able to capture low-frequency entropic modes even without mean-flow terms in the fluctuating-pressure equation.

1. Introduction

In reacting flows, the unsteady heat release rate is a source of acoustic-pressure fluctuations [1]. Under specific conditions, a constructive coupling between combustion and acoustics can lead to sustained oscillations [2] that may reach considerable amplitudes because of the large power density of chemical reactions. This unstable behaviour is called *combustion instability* and virtually all kinds of combustion engines such as gas-turbines, aeronautical turbines or rocket engines experience them at some stage of their design or life-cycle. Combustion instabilities have many undesirable effects such as large-amplitude structural vibrations, flame flashback or blowoff, or an abnormally high temperature of the wall of the combustor. The consequences of combustion instabilities range from loss of performance or premature fatigue of materials to a possible mechanical failure or destruction of the system. Consequently, there is a need for a better understanding of combustion instabilities at the fundamental level, but also the development of tools that can predict them at an early design stage. Combustion instabilities are a very broad field and an important review of driving mechanisms may be found in the literature [3–7].

In principle, numerical resolution of the unsteady reacting Navier–Stokes equations allows one to predict combustion instabilities. Several studies using Large Eddy Simulations have shown the potential of this method, even for realistic engine geometries and operating points [8–10]. These results however come at a tremendous computational cost, impractical for the study of design or operating conditions variations. Many strategies are available to devise lower-order methods by

* Corresponding author. Tel.: +33 5 611 930 24; fax: +33 5 611 930 00.
E-mail address: emmanuel.motheau@cerfacs.fr (E. Motheau).

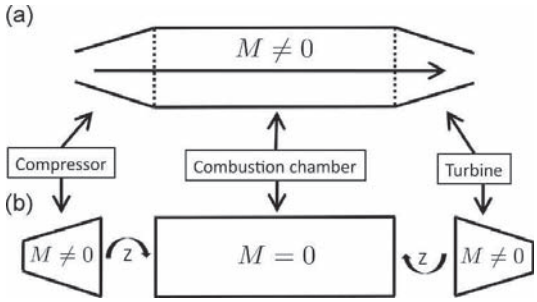

Fig. 1. Schematic view of the proposed modelling strategy. (a) The whole domain is computed while taking the mean flow into account and (b) the combustion chamber is solved under the zero Mach number assumption. The acoustic environment from compressor and turbine is accounted for through impedances.

neglecting viscous terms and through linearisation or reduction to one dimension [11,12]. The Linearised Euler Equations (LEEs) approach gives an accurate representation of the physical thermoacoustic phenomena [13,14] at a reasonable computational cost. However, solving LEE requires numerical schemes that are subject to instability and nonphysical techniques must be used, such as the addition of artificial viscosity [15].

The LEE approach can be further simplified by assuming that the mean flow is at rest, often referred to as the *zero-Mach-number approximation*. Under this assumption, the problem can be reformulated as an inhomogeneous Helmholtz equation for the acoustic pressure. The main advantage of this method is its small computational burden while keeping a realistic geometry. The main drawback is that only acoustic perturbations are accounted for, since vorticity and entropy waves do not propagate when the mean flow is at rest. The effects of convection on the acoustic waves are also neglected. Nevertheless, this method offers great flexibility for physical modelling and systematic variation of input parameters. For example, the flame transfer function that represents flame/acoustic interaction or the acoustic absorption by multiperforated plates have been successfully implemented into a three-dimensional Helmholtz solver [16,17]. Combined with LES, this approach proved useful to gain understanding on the structure and nature of the instabilities observed in a burner [18,19].

When seeking for the thermoacoustic fluctuations in a combustor, the most natural strategy consists in computing the whole engine (cf. Fig. 1a). In this case, one should use the LEE approach because the Mach number, M, is usually not small in the compressor and the turbine. An alternative is to use the Helmholtz approach in the combustion chamber, where $M \ll 1$ while accounting for the upstream and downstream elements through appropriate boundary conditions (cf. Fig. 1b), namely a complex-valued impedance noted Z. These impedances can be deduced from transfer functions describing the response of acoustic elements to acoustic or entropic perturbations, either analytically under the compact hypothesis [20] or numerically by solving the LEE [21].

At least two difficulties arise when using a Helmholtz solver (thus assuming $M=0$) for the combustion chamber and complex impedances as boundary conditions:

- The impedance must be consistent with the zero-Mach-number assumption although it represents an acoustic element where the mean flow is not at rest. Moreover, this impedance must be imposed at a location in the combustion chamber where the Mach number is small.
- As shown by many authors [22–25], entropy fluctuations accelerated in a mean flow generate acoustic waves, which is the case when the combustor opens onto a high pressure distributor. Acoustic waves transmitted through the distributor produce *indirect combustion noise*, while acoustic waves travelling back to the flame may trigger low-frequency resonant modes called *rumble* [26,27]. This important mechanism for combustion instabilities is not accounted for in a Helmholtz solver, since entropy fluctuations do not propagate if the mean flow is at rest.

It has been demonstrated in a previous study [14] that the zero-Mach-number assumption can lead to significant errors for the prediction of both the frequency and the growth rate of combustion instabilities, suggesting that improvements are required for the two items cited above. Since accounting for the non zero-Mach-number terms in the equations leads to a drastic increase in the complexity of the problem [15], the aim of this paper is to propose models that account for these effects in a Helmholtz solver. To this purpose, the basic equations are recalled in Section 2 while in Section 3 two different formulations are proposed in absence of entropy fluctuations. The performance of these formulations is tested in Section 4 by considering a simple configuration. Entropy fluctuations are introduced in Section 5 where we demonstrate that it is possible to account for the coupling between acoustic and entropy waves in a zero-Mach-number framework and to capture a low-frequency mixed mode.

2. Mathematical formalism

This study is conducted in the frequency domain: a fluctuating quantity, $g'(x,t)$, is defined by its complex amplitude, $\hat{g}$, and angular frequency, ω, through $g'(x,t) = \mathrm{Re}\{\hat{g}(x)\mathrm{e}^{-\mathrm{j}\omega t}\}$. The focus is on unidimensional configurations so that only longitudinal

fluctuations are considered. Consequently, vorticity perturbations and their interactions with acoustics are neglected in the remainder of the present paper.

For a homogeneous reacting mixture with constant specific heat capacities C_p and C_v, the linearised harmonic form of conservation equations for mass, momentum and energy in a quasi-1D domain with slowly varying cross section can be found in [14]. In the case of a ducted system with constant-cross-section tubes, it is more practical [28] to describe the fluctuations of pressure, velocity and entropy (respectively $\hat{p}$, $\hat{u}$ and $\hat{s}$) with planar waves of amplitudes A^+ and A^- for the forward and backward propagating acoustic waves, respectively and σ for the entropic wave. One then has

$$\hat{p}(x) = A^+ \mathrm{e}^{\mathrm{j}k^+ x} + A^- \mathrm{e}^{-\mathrm{j}k^- x} \tag{1}$$

$$\hat{u}(x) = \frac{1}{\rho_0 c_0}[A^+ \mathrm{e}^{\mathrm{j}k^+ x} - A^- \mathrm{e}^{-\mathrm{j}k^- x}] \tag{2}$$

$$\hat{s}(x) = \sigma \mathrm{e}^{\mathrm{j}k_s x} \tag{3}$$

where

$$k^+ = \frac{\omega}{c_0 + u_0} = \frac{k}{1+M} \tag{4}$$

$$k^- = \frac{\omega}{c_0 - u_0} = \frac{k}{1-M} \tag{5}$$

$$k_s = \frac{k}{M} \tag{6}$$

and $k = \omega/c_0$ is the acoustic wave number. The entropy equation and perfect-gas equation of state yield

$$\hat{\rho} = \frac{\hat{p}}{c_0^2} - \frac{\rho_0 \sigma}{C_p} \mathrm{e}^{\mathrm{j}k_s x} \quad \text{and} \quad \frac{\hat{T}}{T_0} = \frac{\gamma - 1}{\rho_0 c_0^2} \hat{p} + \frac{\sigma}{C_p} \mathrm{e}^{\mathrm{j}k_s x} \tag{7}$$

Eqs. (1), (2), (3), and (7) describe the linear harmonic perturbations at finite Mach number. These relations will be used in Section 3 to derive consistent boundary conditions between a Helmholtz solver and a finite-Mach-number region and in Section 5 to include the effect of entropy waves in a Helmholtz solver.

3. Consistent boundary conditions from a nonstationary flow to a zero-Mach-number formulation

Following the approach described in Fig. 1b, only the combustion chamber is solved for by using a Helmholtz solver while finite-Mach-number effects in the compressor and/or turbine and/or nozzle are accounted for through boundary conditions by solving either analytically [29] or numerically [21] the LEE. In this section, various ways to chose the impedance at the boundary of the Helmholtz domain are presented. To this purpose, it proves useful to recall how acoustic energy and flux can be defined when dealing with perturbations evolving in a medium at rest or not.

When studying combustion instabilities, the stability is defined by the evolution of the disturbance energy E, which obeys the equation

$$\frac{\partial E}{\partial t} + \nabla \cdot \mathbf{F} = P \tag{8}$$

where $\mathbf{F}$ is the flux of acoustic energy through the boundaries and P is the power of the internal source terms and dissipations [30]. The definition of a proper acoustic energy E is a longstanding problem in the study of combustion instabilities, first addressed by Cantrell and Hart [31] for homentropic, irrotational flows in a cavity, and later extended by Morfey [32] for nonisentropic, heat-conducting viscous flows. A generalisation for arbitrary disturbances in steady flows has been derived by Chu [33] for zero-mean-flow and complemented by Myers [34].

Considering acoustics in the zero-Mach-number limit, one has the following expressions, $E^{M=0}$ and $\mathbf{F}^{M=0}$, specific to the Helmholtz equation:

$$E^{M=0} = \int_0^T \left(\frac{1}{2\rho_0 c_0^2} p'^2 + \frac{\rho_0 u'^2}{2} \right) \mathrm{d}t \tag{9}$$

$$\mathbf{F}^{M=0} = \int_0^T p' u' \, \mathrm{d}t \tag{10}$$

Retaining finite-Mach number effects yields $E^{M\neq 0}$ and $\mathbf{F}^{M\neq 0}$, consistent with the LEE approach:

$$E^{M\neq 0} = \int_0^T \left(\frac{1}{2\rho_0 c_0^2} p'^2 + \frac{\rho_0 u'^2}{2} + \frac{u_0 p' u'}{c_0^2} \right) \mathrm{d}t \tag{11}$$

$$\mathbf{F}^{M\neq 0} = \int_0^T J' m' \, \mathrm{d}t \tag{12}$$

where J' and m' are the linearised isentropic fluctuating parts of the total enthalpy ($J = C_p T + u^2/2$) and the mass flow rate ($m = \rho u$), respectively:

$$J' = \frac{p'}{\rho_0} + u_0 u' \tag{13}$$

$$m' = \rho_0 u' + \frac{u_0}{c_0^2} p' \tag{14}$$

Eq. (10) suggests that the 'natural' variables for a Helmholtz solver are p' and u' while Eq. (12) indicates that J' and m' are more attune for LEE. The choice of this latter set of fluctuating state variables is commonly used in the aeroacoustic community [35,36] because they are themselves independent of the flow when placed in a wave equation, contrary to the pressure or the velocity which are locally dependent on the flow velocity [37]. Moreover, state variables J' and m' are more suitable because their product represents the acoustic power in the presence of a mean flow. However one can notice that these two sets of independent variables are strictly equivalent and one may write the LEE or Helmholtz equations with any set. A reduced impedance, Z, and reflection coefficient, R, may be defined for each set of variables. Using p' and u' one has

$$Z_{p,u} = \frac{p'}{\rho_0 c_0 \, u'} \quad \text{and} \quad R_{p,u} = \frac{A^-}{A^+} \tag{15}$$

while using J' and m' one may define

$$Z_{J,m} = \frac{\rho_0 \, J'}{c_0 m'} \quad \text{and} \quad R_{J,m} = \frac{A^-(1-M)}{A^+(1+M)} \tag{16}$$

where the amplitudes A^+ and A^- have been defined in Eqs. (1) and (2) and represent the propagation/reflection of acoustics waves through/from the LEE domain. The following relation between $Z_{p,u}$ and $Z_{J,m}$ may be derived from Eqs. (13)–(16):

$$Z_{J,m} = \frac{Z_{p,u} + M}{M Z_{p,u} + 1} \tag{17}$$

$$Z_{p,u} = \frac{M - Z_{J,m}}{M Z_{J,m} - 1} \tag{18}$$

The values of the impedances and reflection coefficients for some canonical boundary conditions are recalled in Table 1.

The situation depicted in Fig. 2 where a Helmholtz domain ($M = 0$) is connected to a LEE domain ($M \neq 0$) through an interface raises the question of the consistency between the two sub-domains. More precisely, let us assume that the

Table 1
Impedances and reflection coefficients for canonical boundary conditions: constant pressure ($\hat{p} = 0$), constant velocity ($\hat{u} = 0$), fixed mass flow rate ($\hat{m} = 0$) and fixed total enthalpy ($\hat{J} = 0$).

B.C	$Z_{p,u}$	$R_{p,u}$	$Z_{J,m}$	$R_{J,m}$
$\hat{p} = 0$	0	-1	M	$-\frac{1-M}{1+M}$
$\hat{u} = 0$	∞	1	$\frac{1}{M}$	$\frac{1-M}{1+M}$
$\hat{J} = 0$	$-M$	$-\frac{1+M}{1-M}$	0	-1
$\hat{m} = 0$	$-\frac{1}{M}$	$\frac{1+M}{1-M}$	∞	1

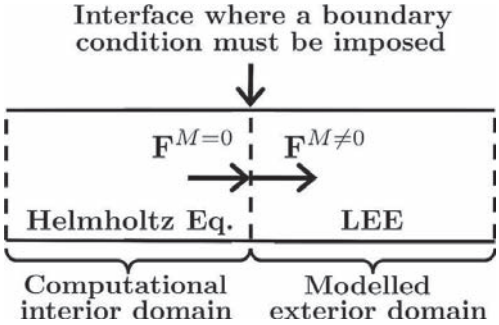

Fig. 2. Schematic representation of the boundary between a domain computed with a Helmholtz solver and a finite Mach number acoustic element.

Table 2
Summary of the flux mismatch error introduced in the zero-Mach number domain by the boundary impedance $Z^{M=0}$ (see Appendix A).

$Z^{M=0}$	$Z_{p,u}^{M\neq 0}$	$Z_{J,m}^{M\neq 0}$
$\lvert\mathbf{F}^{M\neq 0}-\mathbf{F}^{M=0}\rvert$	$\mathcal{O}(M)$	$\mathcal{O}(M^2)$

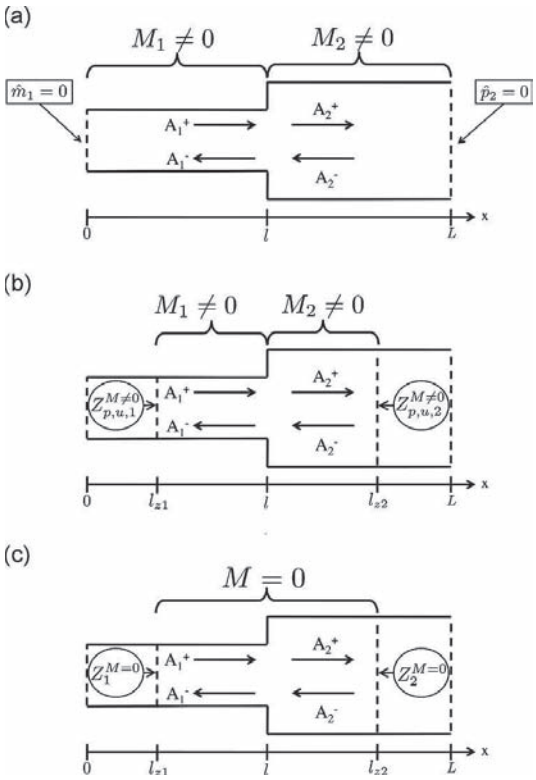

Fig. 3. Configuration investigated in Section 4. (a) Complete geometry with its known acoustic boundary conditions, (b) only a part of the domain is computed while the rest is modelled through impedances and (c) same as (b) but the computed flow domain is assumed at rest.

impedance of the LEE domain is known at the interface, noted $Z_{p,u}^{M\neq 0}$ (or $Z_{J,m}^{M\neq 0}$). This impedance models the way acoustic waves propagate into and reflect from the LEE domain. Since the flow is not at rest in this region, $Z_{p,u}^{M\neq 0}$ and $Z_{J,m}^{M\neq 0}$ are obviously different (Eqs. (17) and (18)) although they represent the same LEE domain. When solving for the Helmholtz equation in the $M=0$ domain, a boundary impedance $Z^{M=0}$ must be imposed at the interface in order to represent the effect of the LEE domain. Note that in the Helmholtz domain the Mach number is assumed zero so that from Eqs. (17) and (18): $Z^{M=0}=Z_{p,u}^{M=0}=Z_{J,m}^{M=0}$. The next natural question is then: how should $Z^{M=0}$ be defined from the knowledge of $Z_{p,u}^{M\neq 0}$ (or $Z_{J,m}^{M\neq 0}$)?

Two approaches for the choice of the boundary impedance $Z^{M=0}$ are analysed and tested in the remainder of the paper; they correspond to $Z^{M=0}=Z_{p,u}^{M\neq 0}$ and $Z^{M=0}=Z_{J,m}^{M\neq 0}$, respectively. This is summarised in Table 2, which also displays the asymptotic behaviours of the difference between the exact energy flux $\mathbf{F}^{M\neq 0}$ (see Eq. (12)) and its zero-Mach-number counterpart $\mathbf{F}^{M=0}$ (see Eq. (10)). A perfect model for the boundary impedance $Z^{M=0}$ would produce zero difference between these two fluxes, meaning that the acoustic energy leaving the Helmholtz domain equals the amount of energy entering the LEE domain. However, assuming the mean flow being at rest in the computational domain introduces a loss in acoustic energy conservation and a mismatch between $\mathbf{F}^{M=0}$ and $\mathbf{F}^{M\neq 0}$. The theoretical analysis conducted in Appendix A shows that the $Z_{p,u}^{M\neq 0}$ approach produces an error $\lvert\mathbf{F}^{M\neq 0}-\mathbf{F}^{M=0}\rvert$ proportional to the Mach number between the Helmholtz and the LEE domains (noted $\mathcal{O}(M)$ in Table 2). At the same time, the $Z_{J,m}^{M\neq 0}$ approach produces a flux mismatch which is quadratic in the Mach number ($\lvert\mathbf{F}^{M\neq 0}-\mathbf{F}^{M=0}\rvert=\mathcal{O}(M^2)$), thus a smaller error in the acoustic energy conservation. These theoretical results are supported by the numerical tests described in Section 4.

4. Application to a simple configuration

The configuration considered is shown in Fig. 3a. It consists of two connected tubes of section S_1 and S_2. The subscripts 1 and 2 refer to parameters in the left and right tubes, respectively. The boundary conditions are $\hat{m}_1=0$ and $\hat{s}_1=0$ at the

Table 3
Summary of the analytical procedures (methods I and II) investigated to compute the two connected tubes configuration.

Method	Computed domain	Mean flow assumption	Impedance formulation (Z_1 and Z_2)
I	Truncated	$M \neq 0$	$Z_{p,u}^{M\neq 0}$
II_{pu}	Truncated	$M=0$	$Z_{p,u}^{M\neq 0}$
II_{Jm}	Truncated	$M=0$	$Z_{J,m}^{M\neq 0}$

entrance of tube 1 and $\hat{p}_2 = 0$ at the exit of tube 2, respectively. This simple test case is chosen so as to mimic a burner where the inlet and outlet Mach numbers are different, but without entropy sources at all so as to keep the isentropic assumption.

4.1. Analytical procedures

The eigenmodes of this simple configuration are computed by two different methods:

- Method I is the analytical solution of the LEE equations in a restricted region of the domain (Fig. 3b) while the rest is modelled through impedances. This solution is considered as the reference solution.
- Method II is the solution of the Helmholtz equation (i.e. assuming that $M=0$) in a restricted region of the domain (Fig. 3b). This solution assesses the influence of the zero-Mach-number assumption and is used to test the two modelling approaches of $Z^{M=0}$ which are summarised in Table 2. To this end, two versions of Method II are used in the following: II_{pu} when $Z^{M=0} = Z_{pu}^{M\neq 0}$ and II_{Jm} when $Z^{M=0} = Z_{Jm}^{M\neq 0}$.

Table 3 summarises the analytical procedures described above.

4.2. Method I: Truncated analytical acoustic model at $M \neq 0$

As shown in Fig. 3b the computational domain is reduced to the region between $x = l_{z1}$ and $x = l_{z2}$, where specific boundary impedances $Z_{p,u,1}^{M\neq 0}$ and $Z_{p,u,2}^{M\neq 0}$ are imposed at these locations. The Mach number remains finite in the computational domain. The forward and backward waves (*cf.* Eqs. (1) and (2)) traveling in both tubes lead to four unknown: A_1^+, A_1^-, A_2^+ and A_2^-. These wave amplitudes are solutions of a homogeneous linear system of equations obtained by requiring that the boundary conditions ($x = l_{z1}$ and $x = l_{z2}$) and jump condition ($x=l$) are fulfilled.

As explained by Davies [28] the jump relations for the section change located at $x=l$ can be expressed by integrating over an infinitesimal control volume the conservation of mass and energy as long as the specific stagnation enthalpy within the volume remains invariant. It should be noted that the physics at the section change involves an additional equation that introduces the entropy fluctuations. However it has been checked by solving numerically the full set of LEE that in the present configuration the generated entropy wave is negligible. As pointed out by Davies [28] in the case of an isentropic processes, the jump relations reduces to the following set of equations:

- Mass conservation at $x=l$:

$$[(1+M_1)A_1^+ \mathrm{e}^{\mathrm{j}k_1^+ l} - (1-M_1)A_1^- \mathrm{e}^{-\mathrm{j}k_1^- l}]\frac{S_1}{c_1} = [(1+M_2)A_2^+ \mathrm{e}^{\mathrm{j}k_2^+ l} - (1-M_2)A_2^- \mathrm{e}^{-\mathrm{j}k_2^- l}]\frac{S_2}{c_2}. \tag{19}$$

- Energy conservation at $x=l$:

$$[(1+M_1)A_1^+ \mathrm{e}^{\mathrm{j}k_1^+ l} + (1-M_1)A_1^- \mathrm{e}^{-\mathrm{j}k_1^- l}]\frac{1}{\rho_1} = [(1+M_2)A_2^+ \mathrm{e}^{\mathrm{j}k_2^+ l} + (1-M_2)A_2^- \mathrm{e}^{-\mathrm{j}k_2^- l}]\frac{1}{\rho_2} \tag{20}$$

The impedances $Z_{p,u,1}^{M\neq 0}$ and $Z_{p,u,2}^{M\neq 0}$ properly represent the truncated regions $0 \le x \le l_{z1}$ and $l_{z2} \le x \le L$. Recall that the boundary conditions are $\hat{m}_1 = 0$ at $x=0$ and $\hat{p}_2 = 0$ at $x=L$, a simple calculation leads to

$$Z_{p,u,1}^{M\neq 0} = \frac{\zeta_1(M_1-1)-(M_1+1)}{\zeta_1(M_1-1)+(M_1+1)} \tag{21}$$

$$Z_{p,u,2}^{M\neq 0} = \frac{1-\zeta_2}{1+\zeta_2} \tag{22}$$

where

$$\zeta_1 = \mathrm{e}^{2\mathrm{j}k_1 l_{z1}/1-M_1^2} \quad \text{and} \quad \zeta_2 = \mathrm{e}^{2\mathrm{j}k_2 l_{z2}/1-M_2^2}. \tag{23}$$

Eqs. (19)–(22) are recast in the form of a linear system $\mathbf{MW}=0$, with

$$\mathbf{M}=\begin{bmatrix} \frac{S_1}{c_1}(1+M_1)e^{jk_1^+ l} & -\frac{S_1}{c_1}(1-M_1)e^{-jk_1^- l} & -\frac{S_2}{c_2}(1+M_2)e^{jk_2^+ l} & \frac{S_2}{c_2}(1-M_2)e^{-jk_2^- l} \\ (1+M_1)\frac{\rho_2}{\rho_1}e^{jk_1^+ l} & (1-M_1)\frac{\rho_2}{\rho_1}e^{-jk_1^- l} & -(1+M_2)e^{jk_2^+ l} & -(1-M_2)e^{-jk_2^- l} \\ (1-Z_{p,u,1}^{M\neq 0})e^{jk_1^+ l_{z1}} & (1+Z_{p,u,1}^{M\neq 0})e^{-jk_1^- l_{z1}} & 0 & 0 \\ 0 & 0 & (1-Z_{p,u,2}^{M\neq 0})e^{jk_2^+ l_{z2}} & (1+Z_{p,u,2}^{M\neq 0})e^{-jk_2^- l_{z2}} \end{bmatrix} \tag{24}$$

and $\mathbf{W}=(A_1^+, A_1^-, A_2^+, A_2^-)^T$ contains the four unknowns. The dispersion relation is then obtained by requiring the matrix $\mathbf{M}$ to be singular, producing the exact solution of the acoustical problem.

4.3. Method II: Truncated analytical acoustic model at $M=0$

Method II is similar to method I in the sense that only the $l_{z1} \le x \le l_{z2}$ domain is solved for. However, the Mach number is now assumed to be zero in this region, so that the $Z^{M=0}$ approximations (see Table 2) can be tested. Methods II_{pu} or II_{Jm} are obtained by replacing $Z_1^{M=0}$ and $Z_2^{M=0}$ by $Z_{p,u,1}^{M\neq 0}$ and $Z_{p,u,2}^{M\neq 0}$, or $Z_{J,m,1}^{M\neq 0}$ and $Z_{J,m,2}^{M\neq 0}$, respectively. The solution of this problem corresponds to the linear system (25).

$$\begin{bmatrix} \frac{S_1}{c_1}e^{jk_1 l} & -\frac{S_1}{c_1}e^{-jk_1 l} & -\frac{S_2}{c_2}e^{jk_2 l} & \frac{S_2}{c_2}e^{-jk_2 l} \\ \frac{\rho_2}{\rho_1}e^{jk_1 l} & \frac{\rho_2}{\rho_1}e^{-jk_1 l} & -e^{jk_2 l} & -e^{-jk_2 l} \\ (1-Z_1^{M=0})e^{jk_1 l_{z1}} & (1+Z_1^{M=0})e^{-jk_1 l_{z1}} & 0 & 0 \\ 0 & 0 & (1-Z_2^{M=0})e^{jk_2 l_{z2}} & (1+Z_2^{M=0})e^{-jk_2 l_{z2}} \end{bmatrix} \begin{bmatrix} A_1^+ \\ A_1^- \\ A_2^+ \\ A_2^- \end{bmatrix} = 0 \tag{25}$$

4.4. Results

Thermodynamic and geometric parameters for the computation of the eigenmodes are presented in Table 4. The temperature T_1 and pressure p_1 are imposed, while the values in tube 2 are deduced from the conservation equations of the steady state.

4.4.1. Effect of the truncation

The objective of this section is to demonstrate the validity of the computations in the truncated domain by comparing method I with the computation of the whole domain. This can be done by simply replacing the two last line of the matrix at Eq. (24) by the following boundary conditions (taking $l_{z1}=0$ and $l_{z2}=L$ in Eqs. (21) and (22)):

$$A_1^+(1+M_1)-A_1^-(1-M_1)=0 \quad \hat{m}_1=0 \text{ at } x=0 \tag{26}$$

$$A_2^+ e^{jk_2^+ L}+A_2^- e^{-jk_2^- L}=0 \quad \hat{p}_2=0 \text{ at } x=L \tag{27}$$

The frequency and growth rate of the first eigenmode are reported in Fig. 4. As the results are identical, this demonstrates that the impedances at $x=l_{z1}$ and $x=l_{z2}$ (Eqs. (21) and (22)) are correct.

The eigenmode shapes were also verified to be identical although not reported here. The present analytical methods were also successfully compared to a numerical LEE solver for the same test case in a previous work by the authors [38], suggesting that the isentropic jump relations (Eqs. (19)–(20)) are valid. This demonstrates that the differences between methods I and II discussed in the next section are due to the zero-Mach-number assumption and the modelling of the boundary impedances rather than the truncation procedure.

4.4.2. Effect of the zero-Mach-number assumption

This section is devoted to the comparison of the methodologies, presented in Section 3, to prescribe the boundary impedances in method II. The reference is the computation using method I. The frequency and growth rate of the first two eigenmodes are reported in Fig. 5 for various inlet Mach number M_1.

Results with the zero-Mach-number assumption methods II_{pu} and II_{Jm} exhibit the same behaviour for the two computed eigenmodes. The frequency of oscillations departs from the reference solution when M_1 increases. This result was expected since a simple reasoning in a constant cross section area tube shows that the frequency of oscillation at $M\neq 0$ is approximatively

Table 4
Thermodynamic and geometric parameters for the computation of the configuration of Fig. 3.

S_1 (m^2)	S_2 (m^2)	T_1 (K)	p_1 (Pa)	γ	r (SI)	L (m)	l (m)	l_{z1} (m)	l_{z2} (m)
0.05	0.1	300	101,325	1.4	287	1	0.5	0.1	0.9

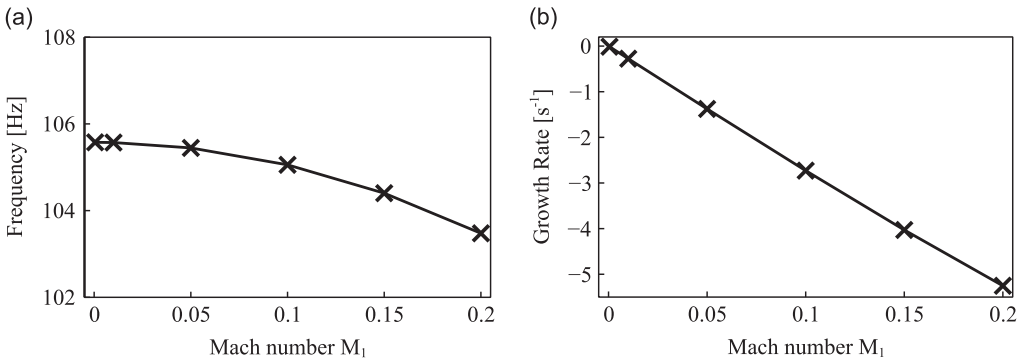

Fig. 4. Frequency (a) and growth rate (b) of the first eigenmode for different inlet Mach number M_1 for the computation of the global domain (×) and the truncated method ($M \neq 0$) I (——).

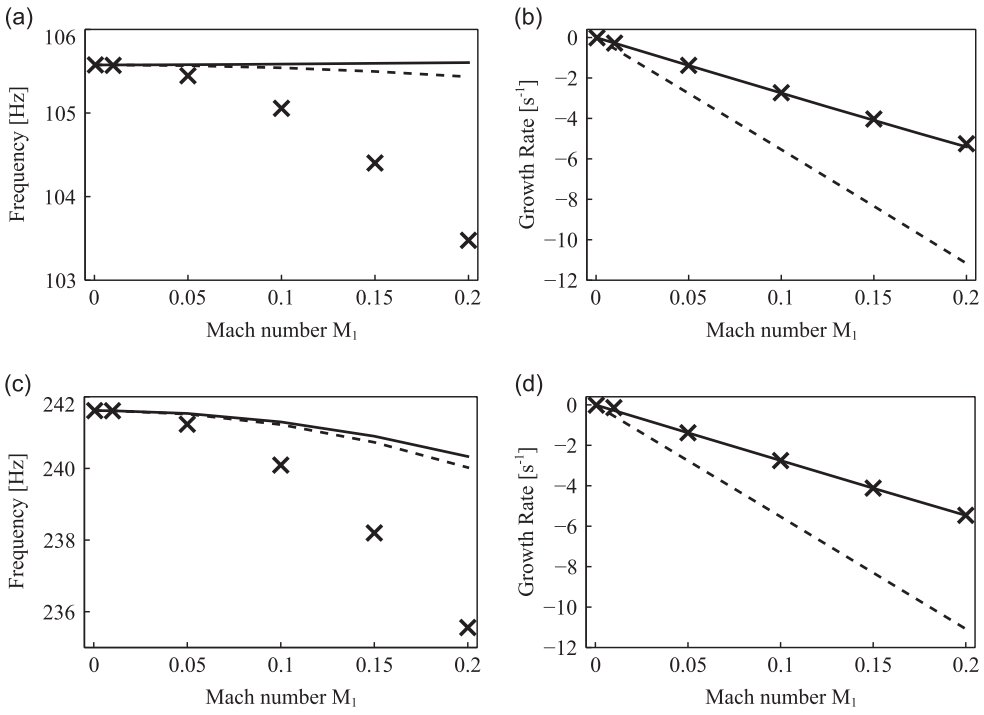

Fig. 5. Frequency and growth rate of the first ((a) and (b)) and second ((c) and (d)) eigenmode versus inlet Mach number M_1 with the reference method I (×) and methods II_{pu} (- - -) and II_{Jm} (——).

$(1-M^2)f_0$ where f_0 is the frequency of oscillation under the zero-Mach-number assumption. The growth rate is significantly underpredicted with method II_{pu} but very well captured by method II_{Jm}. This last result is coherent with the asymptotic behaviours of the flux mismatch presented in Section 3: the method leading to the smallest mismatch (II_{Jm}) also leads to the best result in terms of damping rate.

In order to confirm the theoretical assessment of the flux mismatches introduced by methods II_{pu} and II_{Jm}, viz. $\mathcal{O}(M)$ and $\mathcal{O}(M^2)$ respectively, the flux difference at the boundaries $x = l_{z1}$ and $x = l_{z2}$ is plotted in Fig. 6 for the two first eigenmodes (top and bottom graphs, respectively). As explained in Appendix A, the energy flux are made nondimensional with respect to $\hat{m}_0$, which is taken at $x = l_{z1}$ and $x = l_{z2}$ for the left and right $\Delta\mathbf{F}$, respectively. As expected, the difference between the exact energy flux $\mathbf{F}^{M\neq 0}$ computed with method I and the estimated energy flux $\mathbf{F}^{M=0}$ computed with II_{pu} exhibit an asymptotic behaviour $\mathcal{O}(M)$ while II_{Jm} leads to $\mathcal{O}(M^2)$. This is especially noticeable in Fig. 6 by the use of a log–log frame. The behaviour of the $\Delta\mathbf{F}$ term with methods II_{pu} and II_{Jm} and for different Mach number M_1 is close to the theoretical asymptotic curves with slopes equal to 1 and 2, respectively.

Eigenmode shapes computed at $M_1 = 0.0005$ and $M_1 = 0.2$ are depicted on the left and right columns of Fig. 7, respectively. The first two rows present the modulus and phase of the fluctuating total enthalpy $\hat{J}$, respectively, while the last two rows present the modulus and phase of the fluctuating mass flow rate $\hat{m}$, respectively. All data are made nondimensional by setting $\max(\hat{m}) = 1$. As expected, for the low Mach number case, method II_{Jm} gives the same results as the reference method I. For a larger Mach number $M_1 = 0.2$, method II_{Jm} still gives satisfying results, despite small errors in the estimation of the phase shift.

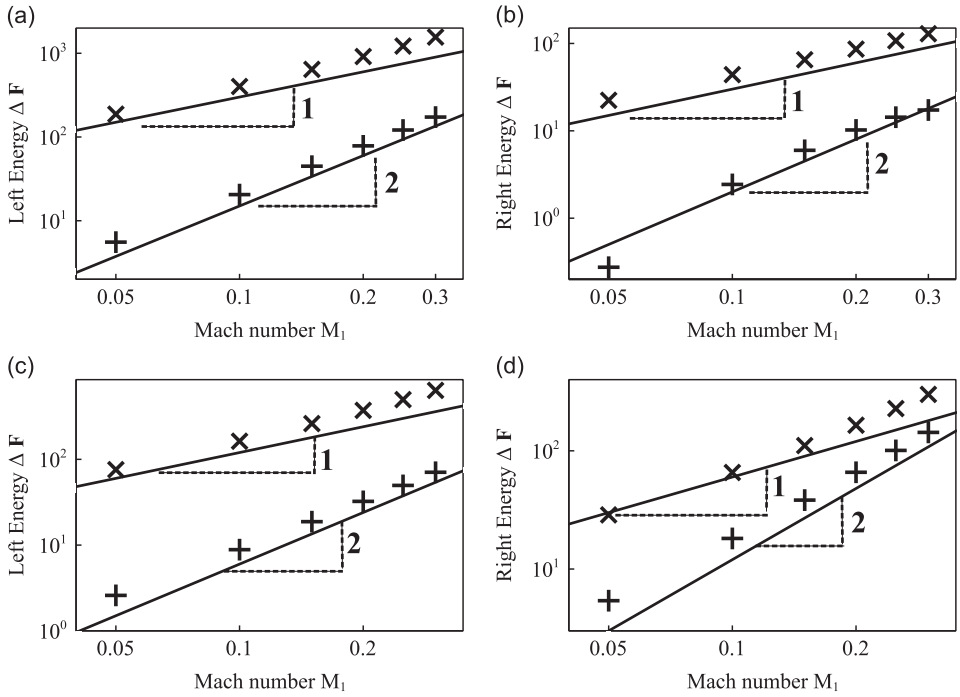

Fig. 6. Flux difference $\Delta\mathbf{F}$ between reference method I and methods II_{pu} (×) and II_{Jm} (+) versus inlet Mach number M_1 and for the first (top) and second (bottom) eigenmode at locations l_{z1} (left) and l_{z2} (right). The theoretical asymptotic behaviour of $\Delta\mathbf{F}$ is illustrated by the solid lines (——) with slopes equal to 1 and 2.

The present study gives a more precise insight about the use of impedances issued from a nonzero-mean-flow framework. The theory of the energy flux conservation indicates that using a formulation which neglects the mean flow (method II_{pu}) leads to significant errors, because the error on the imposed energy flux is $\mathcal{O}(M)$. This statement goes against the previous assumption of Lamarque and Poinsot [21] that prescribed the use of a boundary condition formulated with purely acoustic state variables $\hat{p}$ and $\hat{u}$. As discussed by Peters et al. [35], many authors in the aeroacoustic community prescribe the use of a so-called *energetical* correction of the reflection coefficient which is the $(1-M)/(1+M)$ term in Eq. (16). This term originates from the fact that forward and backward waves do not propagate at the same speed and is directly found in the formulations of acoustical reflection coefficients of ducted flow with area-expansion and/or outside radiation conditions [39,40]. To the authors knowledge, although method II_{Jm} is equivalent to this well-known correction, a detailed analysis of its effect when performing a zero-Mach-number analysis of thermoacoustic modes has not been provided before. The present study shows that a nonzero-Mach-number element can simply be taken into account in a zero-Mach-number framework by using method II_{Jm}. It has been shown that this latter method introduces an error of $\mathcal{O}(M^2)$ and is a good approximation to well capture the growth rate and the shapes of eigenmodes at different frequencies. The following section is devoted to the modelling of the coupling between the acoustic and entropy waves through the extension of method II_{Jm}.

5. Accounting for entropy convection in a zero Mach mean flow

The generation of acoustic waves when entropy inhomogeneities are accelerated in a nonuniform flow is a well known phenomenon that has been extensively studied over the past decades. Early analytical investigations deal with the development of the jet noise theory, extending the work of Lighthill [41] to nonuniform-density flows [22–24]. However these analytical solutions were limited to low-Mach-number flows and focused on the derivation of a formulation for the far field sound radiation into free space by inhomogeneities swept out of an orifice. In a different way, Marble and Candel [20] proposed a one-dimensional theory based on the compact assumption (the nozzle dimensions are small in comparison with the shortest wave length that appears in the flow field). The nozzle may be viewed as a duct discontinuity and simple jump conditions between upstream/downstream acoustic and entropy waves can be written. The recent work of Leyko et al. [42] proposes a comparison of this theory with experiments.

The effect of the presence of a nozzle at the combustor exit on combustion instabilities is not obvious. As reviewed by Hield et al. [43], some authors found no difference on the thermoacoustic modes of their combustor whatever the type of exit used, while Macquisten and Dowling [44] reported that a strong low-frequency instability occurred when the open exit was replaced by a choked nozzle. As explained by Hield et al. [43], the behaviour of such an instability depends to the first order on the geometry. The spatial dispersion of entropy fluctuations by the combustor aerodynamics [45] and the constructive/destructive phase dependency [26] play an important role on the establishment of a coupling between acoustic and entropy modes.

The configuration depicted in Fig. 8 has been chosen in order to exhibit the presence of a set of unstable mixed entropic/acoustic modes. As this kind of modes cannot be predicted by a Helmholtz equation, our objective is to propose a simple

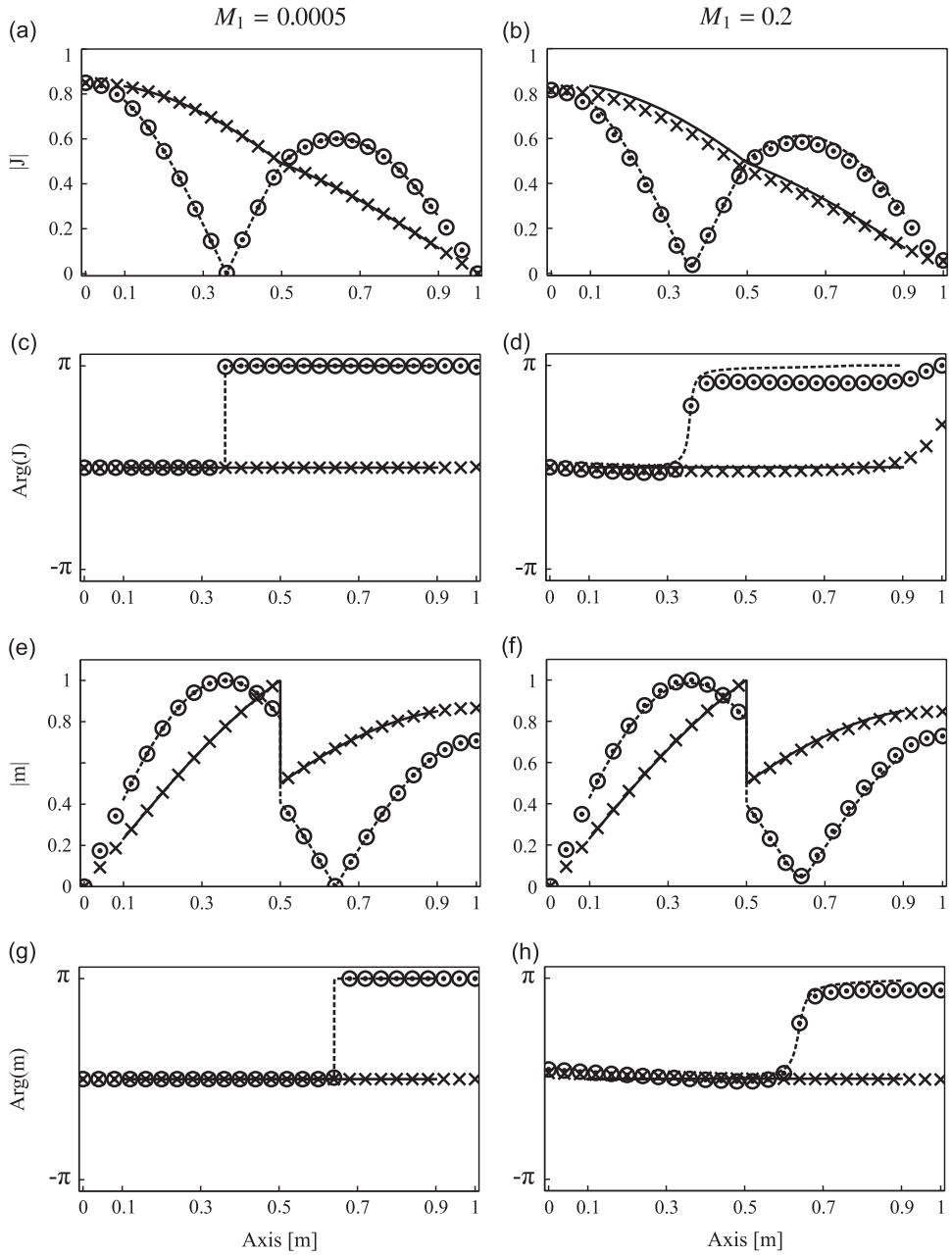

Fig. 7. Mode shapes at $M_1 = 0.0005$ (left column) and $M_1 = 0.2$ (right column) for the first eigenmode with the reference method I (×) and methods II_{Jm} (——), and for the second eigenmode with the reference method I (⊙) and method II_{Jm} (- - -). (a), (b) and (c), (d): Modulus and phase of the fluctuating total enthalpy $\hat{J}$, respectively and (e), (f) and (g), (h): modulus and phase of the fluctuating mass flow rate $\hat{m}$, respectively.

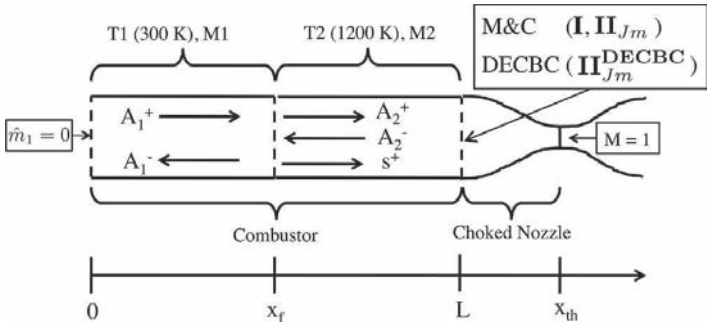

Fig. 8. Configuration investigated in Section 5.

model which, used within the Helmholtz framework, allows predicting mixed entropic/acoustic modes. In a combustion chamber of constant cross section and length L, a compact flame is located at $x=x_f$. A choked nozzle is located at $x=L$ while the sonic throat where the Mach number reaches unity is located at $x=x_{th}$. Following the same methodology as Section 4, this configuration will be computed using three methods.

5.1. *Method I : Truncated analytical thermoacoustic model at $M\neq 0$*

Assuming that the nozzle is properly represented by its acoustic and entropic response at $x=L$, solving the problem presented in Fig. 8 requires six equations for the six unknown wave amplitudes (A_1^+, A_1^-, A_2^+, A_1^-, σ_1 and σ_2). Following the methodology presented by Dowling [11], the following relations can be written:

- Mass conservation translates to

$$\rho_1\hat{u}_1+u_1\hat{\rho}_1=\rho_2\hat{u}_2+u_2\hat{\rho}_2 \tag{28}$$

which is recast into

$$(1+M_1)e^{jk_1^+x_f}A_1^+ +(M_1-1)e^{-jk_1^-x_f}A_1^- -(M_2+1)\frac{c_1}{c_2}e^{jk_2^+x_f}A_2^+ -(M_2-1)\frac{c_1}{c_2}e^{-jk_2^-x_f}A_2^- +M_2\frac{c_1\gamma p_2}{c_2\,C_p}\sigma e^{jk_sx_f}=0 \tag{29}$$

- Momentum conservation yields

$$\hat{p}_1+2\rho_1u_1\hat{u}_1+u_1^2\hat{\rho}_1=\hat{p}_2+2\rho_2u_2\hat{u}_2+u_2^2\hat{\rho}_2 \tag{30}$$

which is recast into

$$(1+M_1)^2e^{jk_1^+x_f}A_1^+ +(M_1-1)^2e^{-jk_1^-x_f}A_1^- -(M_2+1)^2e^{jk_2^+x_f}A_2^+ -(M_2-1)^2e^{-jk_2^-x_f}A_2^- +M_2^2\frac{\gamma p_2}{C_p}\sigma e^{jk_sx_f}=0 \tag{31}$$

- Energy conservation yields

$$C_pT_{01}(\rho_1\hat{u}_1+\hat{\rho}_1u_1)+\rho_1u_1(C_p\hat{T}_1+u_1\hat{u}_1)=C_pT_{02}(\rho_2\hat{u}_2+\hat{\rho}_2u_2)+\rho_2u_2(C_p\hat{T}_2+u_2\hat{u}_2) \tag{32}$$

where $T_{0i}=T_i+\frac{1}{2}u_{0i}^2/C_p$ is the mean stagnation temperature in section i. In terms of wave amplitudes, the energy conservation takes the form:

$$\mathbf{M}_{31}A_1^+ +\mathbf{M}_{32}A_1^- +\mathbf{M}_{33}A_2^+ +\mathbf{M}_{34}A_2^- +M_2^3/2\frac{\gamma p_2}{C_p}\sigma e^{jk_sx_f}=0 \tag{33}$$

where

$$\begin{aligned}
\mathbf{M}_{31}&=\frac{c_1}{c_2}((1+M_1)[M_1+1/(\gamma-1)+M_1^2/2])e^{jk_1^+x_f}\\
\mathbf{M}_{32}&=\frac{c_1}{c_2}((1-M_1)[M_1-1/(\gamma-1)-M_1^2/2])e^{-jk_1^-x_f}\\
\mathbf{M}_{33}&=-((1+M_2)[M_2+1/(\gamma-1)+M_2^2/2])e^{jk_2^+x_f}\\
\mathbf{M}_{34}&=-((1-M_2)[M_2-1/(\gamma-1)-M_2^2/2])e^{-jk_2^-x_f}
\end{aligned}$$

- Inlet boundary condition: at $x=0$ the mass flow rate is assumed constant, i.e. $\hat{m}_1=0$ and it is assumed that no entropy wave is injected, therefore $\sigma_1=0$. Then using Eqs. (1)–(6) yields

$$(1+M_1)A_1^+ -(1-M_1)A_1^- =0 \tag{34}$$

- Outlet boundary condition: at $x=L$ the supersonic choked nozzle is modelled with the following compact relation derived by Marble and Candel [20]:

$$\frac{\hat{u}_2(L)}{c_2}-\left(\frac{\gamma-1}{2}\right)M_2\frac{\hat{p}_2(L)}{\gamma p_2}-\frac{1}{2}M_2\frac{\hat{s}_2(L)}{C_p}=0 \tag{35}$$

Using the wave amplitudes defined in Eqs. (1)–(6), Eq. (35) takes the form:

$$(1-Z_{p,u,2}^{M\neq 0})A_2^+\,e^{jk_2^+L}+(1+Z_{p,u,2}^{M\neq 0})A_2^-e^{-jk_2^-L}-R_{sa}(1+Z_{p,u,2}^{M\neq 0})e^{jk_sL}\frac{\gamma p_2}{C_p}\sigma e^{jk_sL}=0 \tag{36}$$

where $Z_{p,u,2}^{M\neq 0}$ is the impedance of the nozzle submitted to an incident acoustic wave:

$$Z_{p,u,2}^{M\neq 0}=\frac{2}{(\gamma-1)M_2} \tag{37}$$

and R_{sa} is its acoustic response when submitted to a purely entropic perturbation:

$$R_{sa} = -\frac{M_2}{2+(\gamma-1)M_2} \tag{38}$$

Eqs. (30)–(36) may be recast in the form of a linear system $\mathbf{MW} = 0$, where:

$$\mathbf{M} = \begin{bmatrix} (1+M_1)e^{jk_1^+ x_f} & (M_1-1)e^{-jk_1^- x_f} & -(M_2+1)\frac{c_1}{c_2}e^{jk_2^+ x_f} & -(M_2-1)\frac{c_1}{c_2}e^{-jk_2^- x_f} & M_2\frac{c_1}{c_2} \\ (1+M_1)^2 e^{jk_1^+ x_f} & (M_1-1)^2 e^{-jk_1^- x_f} & -(M_2+1)^2 e^{jk_2^+ x_f} & -(M_2-1)^2 e^{-jk_2^- x_f} & M_2^2 \\ \mathbf{M}_{31} & \mathbf{M}_{32} & \mathbf{M}_{33} & \mathbf{M}_{34} & \frac{M_2^3}{2} \\ (1+M_1) & -(1-M_1) & 0 & 0 & 0 \\ 0 & 0 & (1-Z_{p,u,2}^{M\neq 0})e^{jk_2^+ L} & (1+Z_{p,u,2}^{M\neq 0})e^{-jk_2^- L} & -R_{sa}(1+Z_{p,u,2}^{M\neq 0})e^{jk_s(L-x_f)} \end{bmatrix} \tag{39}$$

and $\mathbf{W} = (A_1^+, A_1^-, A_2^+, A_2^-, \Sigma)^T$, with $\Sigma = \gamma p_2 \sigma / C_p e^{jk_s x_f}$. The corresponding dispersion relation is obtained by zeroing det (**M**).

5.2. Method II_{Jm} : Truncated analytical thermoacoustic model at $M=0$

Assuming that $M=0$ imposes that there is no entropic wave, i.e. $\sigma_1 = \sigma_2 = 0$. The 5-by-5 linear system in Eq. (39) reduces to a 4-by-4 system:

$$\begin{bmatrix} \frac{e^{jk_1 x_f}}{\rho_1 c_1} & -\frac{e^{-jk_1 x_f}}{\rho_1 c_1} & -\frac{e^{jk_2 x_f}}{\rho_2 c_2} & \frac{e^{-jk_2 x_f}}{\rho_2 c_2} \\ e^{jk_1 x_f} & -e^{-jk_1 x_f} & -e^{jk_2 x_f} & -e^{-jk_2 x_f} \\ 1 & -1 & 0 & 0 \\ 0 & 0 & (1-Z_{J,m,2}^{M\neq 0})e^{jk_2 L} & (1+Z_{J,m,2}^{M\neq 0})e^{-jk_2 L} \end{bmatrix} \begin{bmatrix} A_1^+ \\ A_1^- \\ A_2^+ \\ A_2^- \end{bmatrix} = 0 \tag{40}$$

Only method II_{Jm} is used in this section given its better behaviour compared to method II_{pu} (see Section 3). Thus, at $x=0$ the boundary condition $\hat{m}_1 = 0$ leads to $Z_{J,m,1}^{M\neq 0} = \infty$ (see Table 2), which may be written into the relation $A_1^+ - A_1^- = 0$. At $z=L$ the impedance $Z_{J,m,2}^{M\neq 0}$ may be expressed with Eqs. (17) and (37), leading to

$$Z_{J,m,2}^{M\neq 0} = \frac{1}{M_2}\frac{1+(\gamma-1)M_2^2/2}{1+(\gamma-1)/2} \tag{41}$$

5.3. Method $\mathrm{II}_{Jm}^{\mathrm{DECBC}}$: "delayed entropy coupled boundary condition"

The formalism of method II_{Jm} is used so as to handle properly the acoustic energy flux that arises from the nozzle connected to the domain computed under the zero-Mach-number assumption. However it does not represent the entropy/acoustic coupling since $\hat{s}$ is set to zero in agreement with the zero-Mach-number assumption. This is the objective of the DECBC approach: model the effect of the accelerated entropy fluctuations on acoustics within the zero-Mach-number region. To this purpose, the entropy fluctuations caused by the flame are modelled first and then analytically convected downstream.

Combining Eqs. (7), (28), (32) and taking the limit $u_2 \to 0$ while the product $u_2\hat{s}$ remains finite [11], one obtains the following expression for the entropy produced by the flame at $x = x_f$:

$$\hat{s}_2(x_f) = -\frac{C_p^2(T_{02}-T_{01})(\gamma-1)\rho_1}{u_2 c_2^2}\frac{}{\rho_2}\hat{u}_1(x_f) \tag{42}$$

Entropy fluctuations at the exit $x=L$ may be analytically expressed by the addition of a time delay that mimics the convection of the entropy fluctuations by the mean flow:

$$\hat{s}_2(L) = \hat{s}_2(x_f)e^{j\omega\tau_s} \quad \text{with } \tau_s = \frac{L-x_f}{u_2} \tag{43}$$

Injecting Eq. (43) into Eq. (36), and expressing $\hat{u}_1(x_f)$ in terms of waves A_1^+ and A_1^- allows us to write the following condition at $x=L$:

$$A_1^+ e^{jk_1 x_f}(\beta R_{sa}(1+Z_{J,m,2}^{M\neq 0})) - A_1^- e^{-jk_1 x_f}(\beta R_{sa}(1+Z_{J,m,2}^{M\neq 0})) + A_2^+ e^{jk_2 L}(1-Z_{J,m,2}^{M\neq 0}) + A_2^+(1+Z_{J,m,2}^{M\neq 0})e^{-jk_2 L} = 0 \tag{44}$$

with

$$\beta = \frac{1}{2}\frac{C_p(T_2-T_1)(\gamma-1)e^{j\omega\tau_s}}{u_2 c_1} \tag{45}$$

Table 5
Thermodynamic parameters for the computation of the configuration in Fig. 8.

T_1 (K)	p_1 (Pa)	T_2 (K)	γ	r (SI)	L (m)	x_f (m)	x_{th} (m)
300	101,325	1200	1.4	287	1	0.75	1.0087

The contribution of the DECBC method appears in the two first terms of Eq. (44), by coupling acoustic waves at the boundary condition ($x=L$) with the acoustic waves upstream of the flame. Finally, the 5×5 problem defined in Eq. (39) reduces to Eq. (46):

$$\begin{bmatrix} \frac{e^{jk_1x_f}}{\rho_1c_1} & -\frac{e^{-jk_1x_f}}{\rho_1c_1} & -\frac{e^{jk_2x_f}}{\rho_2c_2} & \frac{e^{-jk_2x_f}}{\rho_2c_2} \\ e^{jk_1x_f} & -e^{-jk_1x_f} & -e^{jk_2x_f} & -e^{-jk_2x_f} \\ 1 & -1 & 0 & 0 \\ \beta R_{sa}(1+Z^{M\neq0}_{J,m,2})e^{jk_1x_f} & -\beta R_{sa}(1+Z^{M\neq0}_{J,m,2})e^{-jk_1x_f} & (1-Z^{M\neq0}_{J,m,2})e^{jk_2L} & (1+Z^{M\neq0}_{J,m,2})e^{-jk_2L} \end{bmatrix} \begin{bmatrix} A_1^+ \\ A_1^- \\ A_2^+ \\ A_2^- \end{bmatrix} = 0 \tag{46}$$

5.4. Results

Thermodynamic parameters used in the computation of eigenmodes of the configuration depicted in Fig. 8 are presented in Table 5. Note that the compact assumption of Marble and Candel [20] has been validated by numerical computation of the LEE on the complete geometry [38].

5.4.1. Frequency analysis

Results are presented in Fig. 9 for various inlet Mach numbers M_1. The upper left graph presents the frequency of the first three eigenmodes predicted by with the reference method I and zero-Mach-number methods II_{Jm} and $\mathrm{II}_{Jm}^{\mathrm{DECBC}}$. The associated growth rates are depicted on the upper right, lower left and lower right graphs, respectively.

The behaviour of the first eigenmode shows a strong dependency on the Mach number. The frequency is proportional to the convective time delay of the flow, suggesting that this first eigenmode is coupled with entropic waves. This eigenmode is not predicted by method II_{Jm}. The second and third eigenmodes do not present the same behaviour and their frequencies do not follow a linear behaviour with respect to M_1. At very small Mach number, the reference solution I and Helmholtz computations with method II_{Jm} give the same estimation of the frequencies. It suggests that the second and third eigenmodes are mostly acoustic, but influenced by their interactions with the mean flow and the coupling with entropy waves at the exit nozzle. Note that when approaching Mach number $M_1=0.05$, the two first eigenmodes tend to merge into a unique unstable mode. Such behaviour has already been observed by Dowling and Stow [46] and Goh and Morgans [47] which computed several academic combustors while taking into account the dissipation and dispersion of the entropy wave. It was shown that the entropy wave can destabilise a stable combustor and vice-versa, and that some configurations can exhibit a *mode switch* between unstable eigenmodes.

As the first eigenmode is purely dependent on the convective time delay, it can obviously not be captured by the Helmholtz solver when using method II_{Jm}. In the same way, the two other eigenmodes computed with II_{Jm} are invariant in frequency whichever the Mach number prescribed, because no convective effect is taken into account. The relative growth rates of the eigenmodes are also very close to zero, suggesting that the stability map of this kind of configuration cannot be estimated with a simple Helmholtz solver.

It is remarkable that the zero-Mach-number method $\mathrm{II}_{Jm}^{\mathrm{DECBC}}$ is able to very well capture the frequency of each eigenmode. By comparison with the reference method I, the behaviour of the growth rate is well estimated, although slightly over-estimated for $M_1 > 0.025$.

5.4.2. Modes shapes analysis

Eigenmode shapes computed at $M_1 = 0.00625$ and $M_1=0.05$ are depicted on left and right columns of Fig. 10 for the second eigenmode. The first two rows present the modulus and phase of the fluctuating total enthalpy $\hat{J}$, respectively, while the last two rows present the modulus and phase of the fluctuating mass flow rate $\hat{m}$, respectively. All data are made nondimensional by setting $\max(\hat{m}) = 1$.

As expected, the zero-Mach-number method II_{Jm} where entropy waves are not taken into account give good results at very low Mach number. At larger Mach numbers, the modes shapes are mispredicted because the frequency is not well predicted and corresponds to the zero-Mach-number solution. However, modes shapes computed with method $\mathrm{II}_{Jm}^{\mathrm{DECBC}}$ are very close to the reference method I. The enthalpy and mass-flow rate jumps across the flame at $x = x_f$ are well captured. The present results show that the use of the DECBC approach is able to capture mixed-modes based on coupling between entropy and acoustics, and to predict them correctly, despite the fact that the mean flow is neglected within the computational domain.

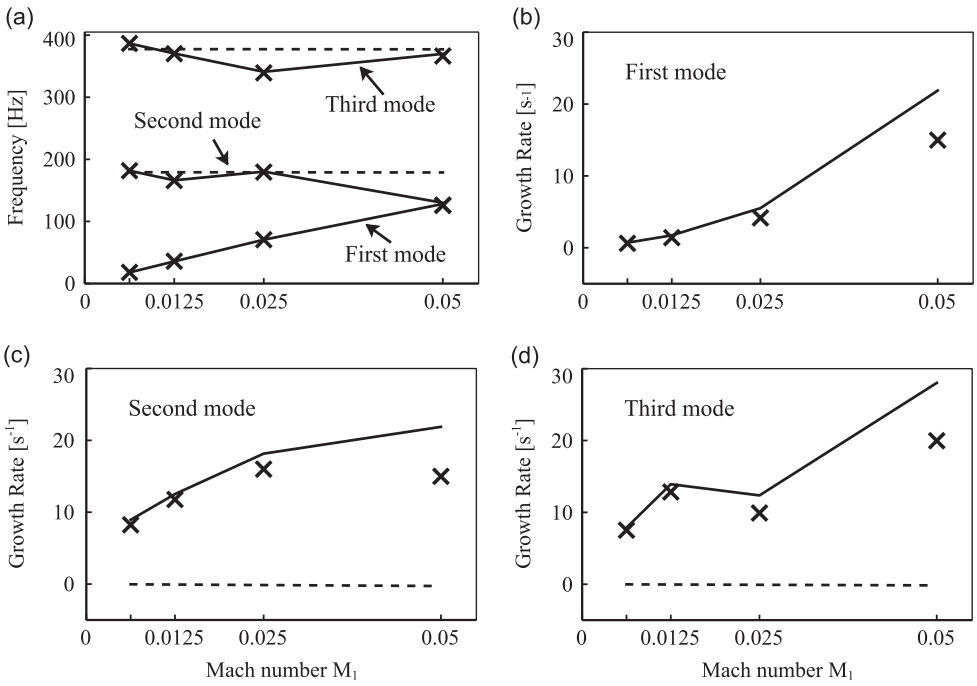

Fig. 9. First three eigenmodes computed with methods I (×), II_{Jm} (- - -) and II_{Jm}^{DECBC} (——) versus inlet Mach numbers M_1. (a) frequency and (b), (c) and (d) growth rate.

5.5. Application to 3D Helmholtz solver

In the present paper, the DECBC methodology is introduced and validated in a 1D analytical framework. The concept is relevant to capture mean flow effects and a family of mixed, convective modes within a zero-Mach-number framework. When dealing with actual configurations, the extension of DECBC to a 3D Helmholtz solver raises several questions:

- Entropy fluctuations at the flame location: In a real configuration, the flame is not a simple 1D interface and the use of Eq. (42) as a model for the entropy fluctuations is highly questionable.
- Characteristic time lag: The convection time between the flame and the nozzle is mostly related to the mean flow velocity in the combustor. However, as real systems feature complex swirled turbulent flows so as to enhance the combustion, this convection time and related dissipation must be assessed carefully.

These points have been preliminary addressed by the authors (see [48,49]) in the case of a realistic aero-engine combustor that features a low-frequency instability relying on a mixed mode. The DECBC framework was coupled to a 3D Helmholtz solver [16] to investigate the possibility to reproduce this low frequency mode. To this purpose, two transfer functions were post-processed from LES snapshots of the configuration and used to feed the Helmholtz/DECBC solver:

- a first one for modelling the entropy fluctuations generated in the flame region from the knowledge of the acoustic fluctuations taken at a reference point in the fresh gas region,
- a second one for modelling the entropy perturbations over the flame to the downstream nozzle.

The 3D Helmholtz solver then proved able to reproduce the mixed, unstable mode that cannot be captured by solving only the Helmholtz equation, showing the potential of the present approach to address realistic combustors.

6. Conclusions

The present study is devoted to the modelling of mean flow effects while computing thermoacoustic eigenmodes under the zero-Mach-number assumption. It has been shown that when the computational domain is represented under the $M=0$ assumption, a nonzero-Mach-number element can simply be taken into account by imposing a proper acoustic impedance at the boundaries so as to mimic the mean flow effects in the outer, not computed flow domain. In this respect, this paper demonstrates that the best way to define the boundary impedance is the use of energetic state variables $\hat{J}$ and $\hat{m}$. This choice introduces an acoustic energy flux mismatch at the $M=0/M\neq 0$ interface proportional to the square of the Mach number,

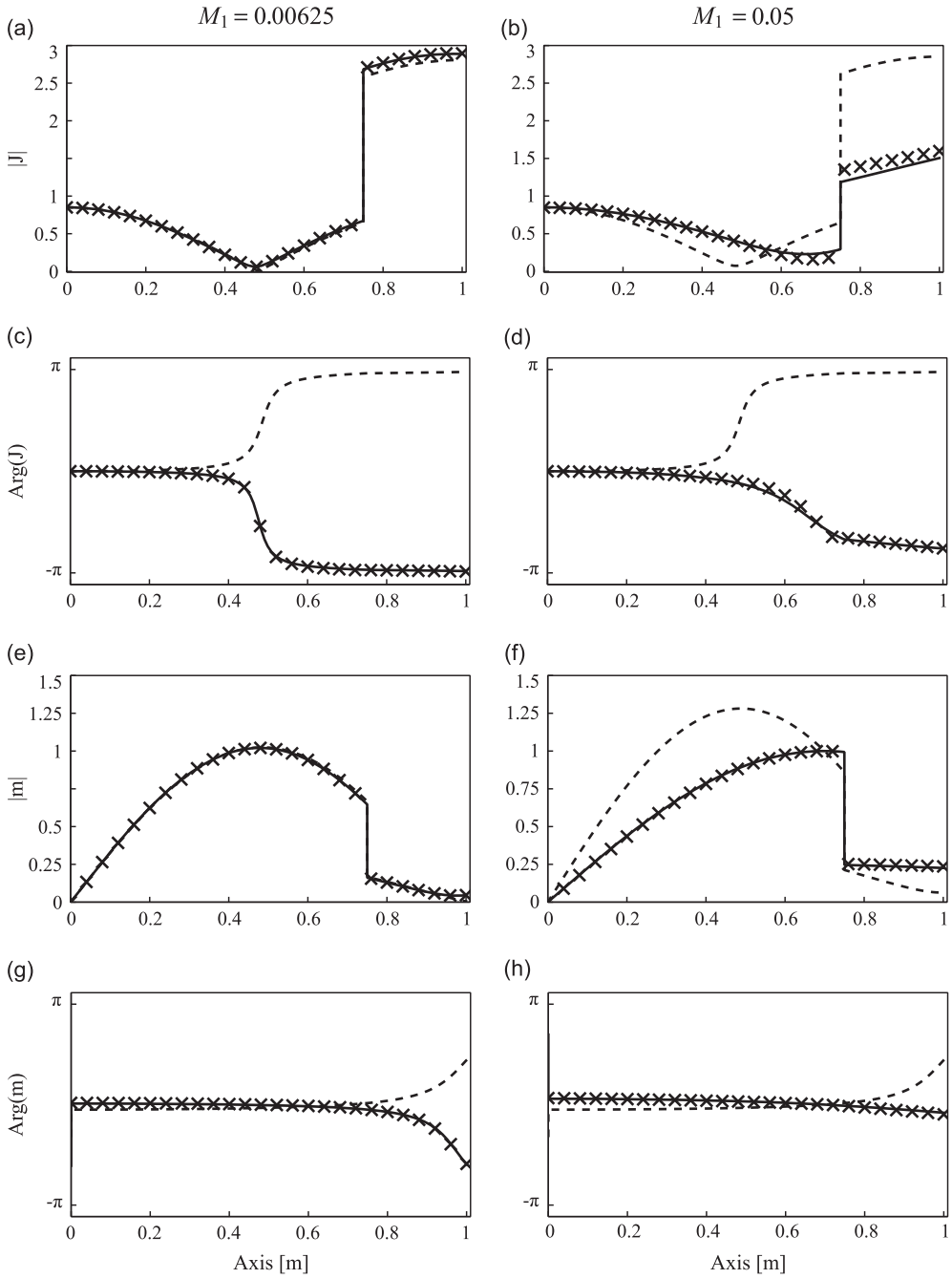

Fig. 10. Mode shapes at $M_1 = 0.0125$ (left column) and $M_1 = 0.05$ (right column) for the second eigenmode with the reference method I (×), method II_{Jm} (- - -) and method II_{Jm}^{DECBC} (——). (a), (b) and (c), (d): Modulus and phase of the fluctuating total enthalpy $\hat{J}$, respectively and (e), (f) and (g), (h): modulus and phase of the fluctuating mass flow rate $\hat{m}$, respectively.

instead of being proportional to M when relying on the acoustic variables $\hat{p}$ and $\hat{u}$. The analytical asymptotic theory has been validated on a simple test case by computing eigenmodes either by solving the Linearised Euler Equation or the zero-Mach-number Helmholtz equation.

The coupling between entropy and acoustic waves at the entrance of a nozzle generates a low frequency eigenmode and a shift of higher frequency modes that does not appear when the convective effects are neglected, namely when using a Helmholtz solver. Such phenomena can be taken into account thanks to the proposed “delayed entropy coupled boundary condition” compatible with a zero-Mach-number formulation. A specific academic test case consisting in a 1D combustion chamber mounted on a compact nozzle is used to illustrate the accuracy of the method.

Although the developments detailed in this paper are illustrated by considering only quasi-1D geometries, they can be extended to 3D configurations. In this respect, these findings are expected to increase the predictive capability of Helmholtz solvers when dealing with realistic thermoacoustic systems, such as industrial gas turbines.

Appendix A

The objective of this appendix is to assess the flux difference $\mathbf{F}^{M\neq 0}-\mathbf{F}^{M=0}$ at the interface between the Helmholtz domain and the outer domain where the baseline flow is not assumed at rest (see Fig. 2). The energy flux $\mathbf{F}^{M\neq 0}$ relative to the LEE domain may be reformulated with the help of the impedance $Z_{J,m}^{M\neq 0}$ defined at Eq. (16). Introducing first the notation $\{\hat{g}\}=\Re(\hat{g}\mathrm{e}^{-\mathrm{j}\omega t})$, Eq. (12) then becomes

$$\mathbf{F}^{M\neq 0}=\int_0^T\{\hat{m}\}\left\{\hat{j}\right\}\mathrm{d}t=\int_0^T\frac{c_0}{\rho_0}\{\hat{m}\}\left\{Z_{J,m}^{M\neq 0}\hat{m}\right\}\mathrm{d}t \tag{A.1}$$

The LEE solution is made nondimensional by setting $\hat{m}=\hat{m}_0$ at the considered boundary, leading to

$$\mathbf{F}^{M\neq 0}=\rho_0 c_0\int_0^T\left\{\frac{\hat{m}_0}{\rho_0}\right\}\left\{Z_{J,m}^{M\neq 0}\frac{\hat{m}_0}{\rho_0}\right\}\mathrm{d}t \tag{A.2}$$

The energy flux $\mathbf{F}^{M=0}$ relative to the zero-Mach number domain may be reformulated with the help of the impedance $Z^{M=0}$. Eq. (10) then becomes

$$\mathbf{F}^{M=0}=\int_0^T\{\hat{u}\}\{\hat{p}\}\,\mathrm{d}t=\rho_0 c_0\int_0^T\{\hat{u}\}\{Z^{M=0}\hat{u}\}\,\mathrm{d}t \tag{A.3}$$

In the Helmholtz domain $\hat{m}=\rho_0\hat{u}$ so that the acoustic field is made nondimensional by setting at the boundary $\hat{u}=\hat{m}_0/\rho_0$. The energy flux $\mathbf{F}^{M=0}$ then becomes

$$\mathbf{F}^{M=0}=\rho_0 c_0\int_0^T\left\{\frac{\hat{m}_0}{\rho_0}\right\}\left\{Z^{M=0}\frac{\hat{m}_0}{\rho_0}\right\}\mathrm{d}t \tag{A.4}$$

The error introduced by the modelling of $Z^{M=0}$ with methods II_{pu} and II_{Jm} (see Section 4) can be assessed by forming the flux difference $\Delta\mathbf{F}=|\mathbf{F}^{M\neq 0}-\mathbf{F}^{M=0}|$ where the flux Eq. (A.2) is used together with Eq. (A.4). Different flux differences are obtained depending on the modelling choice made for $\mathbf{F}^{M=0}$:

- **Method** II_{pu}: The impedance $Z^{M=0}$ is equal to $Z_{p,u}^{M\neq 0}$. Asymptotic expansion with respect to the Mach number leads to

$$Z^{M=0}=Z_{p,u}^{M\neq 0}=\frac{M-Z_{J,m}^{M\neq 0}}{MZ_{J,m}^{M\neq 0}+1}=Z_{J,m}^{M\neq 0}+\mathcal{O}(M) \tag{A.5}$$

  Injection of Eq. (A.5) into Eq. (A.4) leads to the following energy flux formulation for the zero-Mach number domain:

$$\mathbf{F}^{M=0}=\rho_0 c_0\int_0^T\left\{\frac{\hat{m}_0}{\rho_0}\right\}\left\{Z_{J,m}^{M\neq 0}\frac{\hat{m}_0}{\rho_0}\right\}\mathrm{d}t+\mathcal{O}(M) \tag{A.6}$$

  so that, taking the difference between Eqs. (A.(2) and A.6) and keeping only lower order terms, the flux difference is then:

$$\Delta\mathbf{F}=\mathcal{O}(M) \tag{A.7}$$

- **Method** II_{Jm}: The impedance $Z^{M=0}$ is equal to $Z_{J,m}^{M\neq 0}$. Eq. (A.4) then becomes

$$\mathbf{F}^{M=0}=\rho_0 c_0\int_0^T\left\{\frac{\hat{m}_0}{\rho_0}\right\}\left\{Z_{J,m}^{M\neq 0}\frac{\hat{m}_0}{\rho_0}\right\}\mathrm{d}t \tag{A.8}$$

  so that the theoretical flux difference is simply $\Delta\mathbf{F}=0$. However, neglecting the mean flow in the zero-Mach-number domain also introduces a mismatch in the frequency $1/T$ of oscillation of order M^2 (see Section 4.4.2) so that the flux difference is actually:

$$\Delta\mathbf{F}=\mathcal{O}(M^2) \tag{A.9}$$

References

[1] S. Kotake, On combustion noise related to chemical reactions, *Journal of Sound and Vibration* 42 (1975) 399–410.
[2] L. Rayleigh, The explanation of certain acoustic phenomena, *Nature* 18 (July) (1878) 319–321.
[3] S. Candel, Combustion dynamics and control: *progress and challenges*, *Proceedings of the Combustion Institute* 29 (2002) 1–28.
[4] F.E.C. Culick, P. Kuentzmann, *Unsteady Motions in Combustion Chambers for Propulsion Systems*, NATO Research and Technology Organization, 2006.
[5] L. DeGoey, J. van Oijen, V. Kornilov, J. ten ThijeBoonkkamp, Propagation dynamics and control of laminar premixed flames, *Proceedings of the Combustion Institute* 33 (2011) 863–886.
[6] Y. Huang, V. Yang, Dynamics and stability of lean-premixed swirl-stabilized combustion, *Progress in Energy and Combustion Science* 35 (2010) 293–364.
[7] T. Lieuwen, Modeling premixed combustion-acoustic wave interactions: *a review*, *Journal of Propulsion and Power* 19 (2003) 765–781.
[8] H. Pitsch, Large eddy simulation of turbulent combustion, *Annual Review of Fluid Mechanics* 38 (2006) 453–482.
[9] P. Schmitt, T. Poinsot, B. Schuermans, K.P. Geigle, Large-eddy simulation and experimental study of heat transfer, nitric oxide emissions and combustion instability in a swirled turbulent high-pressure burner, *Journal of Fluid Mechanics* 570 (2007) 17–46.

[10] P. Wolf, R. Balakrishnan, G. Staffelbach, L. Gicquel, T. Poinsot, Using LES to study reacting flows and instabilities in annular combustion chambers, *Flow, Turbulence and Combustion* 88 (2012) 191–206.
[11] A.P. Dowling, The calculation of thermoacoustic oscillations, *Journal of Sound and Vibration* 180 (1995) 557–581.
[12] W. Polifke, A. Poncet, C.O. Paschereit, K. Doebbeling, Reconstruction of acoustic transfer matrices by instationnary computational fluid dynamics, *Journal of Sound and Vibration* 245 (2001) 483–510.
[13] Y.C. Yu, J.C. Sisco, V. Sankaran, W.E. Anderson, Effects of mean flow, entropy waves, and boundary conditions on longitudinal combustion instability, *Combustion Science and Technology* 182 (2010) 739–776.
[14] F. Nicoud, K. Wieczorek, About the zero mach number assumption in the calculation of thermoacoustic instabilities, *International Journal of Spray and Combustion Dynamics* 1 (2009) 67–112.
[15] P.P. Rao, P.J. Morris, Use of finite element methods in frequency domain aeroacoustics, *AIAA Journal* 44 (2006) 1643–1652.
[16] F. Nicoud, L. Benoit, C. Sensiau, T. Poinsot, Acoustic modes in combustors with complex impedances and multidimensional active flames, *AIAA Journal* 45 (2007) 426–441.
[17] E. Gullaud, S. Mendez, C. Sensiau, F. Nicoud, T. Poinsot, Effect of multiperforated plates on the acoustic modes in combustors, *Compte Rendu Académie Science* 337 (2009) 406–414.
[18] L. Selle, L. Benoit, T. Poinsot, F. Nicoud, W. Krebs, Joint use of compressible large-eddy simulation and Helmholtz solvers for the analysis of rotating modes in an industrial swirled burner, *Combustion and Flame* 145 (2006) 194–205.
[19] P. Wolf, G. Staffelbach, L.Y.M. Gicquel, J.-D. Müller, T. Poinsot, Acoustic and large eddy simulation studies of azimuthal modes in annular combustion chambers, *Combustion and Flame* 159 (2012) 3398–3413.
[20] F.E. Marble, S. Candel, Acoustic disturbances from gas nonuniformities convected through a nozzle, *Journal of Sound and Vibration* 55 (1977) 225–243.
[21] N. Lamarque, T. Poinsot, Boundary conditions for acoustic eigenmodes computation in gas turbine combustion chambers, *AIAA Journal* 46 (2008) 2282–2292.
[22] C.L. Morfey, Amplification of aerodynamic noise by convected flow inhomogeneities, *Journal of Sound and Vibration* 31 (1973) 391–397.
[23] J.E. Ffowcs Williams, M.S. Howe, The generation of sound by density inhomogeneities in low mach number nozzle flows, *Journal of Fluid Mechanics* 70 (1975) 605–622.
[24] M.S. Howe, Contributions to the theory of aerodynamic sound, with application to excess jet noise and the theory of the flute, *Journal of Fluid Mechanics* 71 (1975) 625–673.
[25] S. Candel, Acoustic conservation principles, application to plane and modal propagation in nozzles and diffusers, *Journal of Sound and Vibration* 41 (1975) 207–232.
[26] W. Polifke, C.O. Paschereit, K. Döbbeling, Constructive and destructive interference of acoustic and entropy waves in a premixed combustor with a choked exit, *International Journal of Acoustics and Vibration* 6 (2001) 135–146.
[27] G.J. Bloxsidge, A.P. Dowling, N. Hooper, P.J. Langhorne, Active control of reheat buzz, *AIAA Journal* 26 (1988) 783–790.
[28] P.O.A.L. Davies, Practical flow duct acoustics, *Journal of Sound and Vibration* 124 (1988) 91–115.
[29] I. Duran, S. Moreau, Solution of the quasi-one-dimensional linearized Euler equations using flow invariants and the Magnus expansion, *Journal of Fluid Mechanics* 723 (2013) 190–231.
[30] T. Poinsot, D. Veynante, *Theoretical and Numerical Combustion*, Third edition, (www.cerfacs.fr/elearning) 2011.
[31] R.H. Cantrell, R.W. Hart, Interaction between sound and flow in acoustic cavities: *mass, momentum, and energy considerations*, *Journal of the Acoustical Society of America* 36 (1964) 697.
[32] C.L. Morfey, Acoustic energy in non-uniform flows, *Journal of Sound and Vibration* 14 (1971) 159–170.
[33] B.T. Chu, On the energy transfer to small disturbances in fluid flow (part i), *Acta Mechanica* (1965) 215–234.
[34] M. Myers, Transport of energy by disturbances in arbitrary steady flows, *Journal of Fluid Mechanics* 226 (1991) 383–400.
[35] M. Peters, A. Hirschberg, A.J. Reijnen, A.P.J. Wijnands, Damping and reflection coefficient measurements for an open pipe at low mach and low Helmholtz numbers, *Journal of Fluid Mechanics* 256 (1993) 499.
[36] M. Karlsson, M. Åbom, Aeroacoustics of t-junctions – an experimental investigation, *Journal of Sound and Vibration* 329 (2010) 1793–1808.
[37] P.E. Doak, Fluctuating total enthalpy as the basic generalized acoustic field, *Theoretical and Computational Fluid Dynamics* 10 (1998) 115–133.
[38] E. Motheau, F. Nicoud, T. Poinsot, Using boundary conditions to account for mean flow effects in a zero mach number acoustic solver, *Journal of Engineering for Gas Turbines and Power* 134 (2012) 111502.
[39] P. Durrieu, G. Hofmans, G. Ajello, R. Boot, Y. Auregan, A. Hirschberg, M.C.A.M. Peters, Quasisteady aero-acoustic response of orifices, *Journal of the Acoustical Society of America* 110 (2001) 1859–1872.
[40] S. Boij, Flow effects on the acoustic end correction of a sudden in-duct area expansion, *Journal of the Acoustical Society of America* 126 (2009) 995–1004.
[41] M.J. Lighthill, On sound generated aerodynamically: *I. general theory*, *Proceedings of the Royal Society of London* 211 (1952) 564–587.
[42] M. Leyko, S. Moreau, F. Nicoud, T. Poinsot, Numerical and analytical modelling of entropy noise in a supersonic nozzle with a shock, *Journal of Sound and Vibration* 330 (2011) 3944–3958.
[43] P.A. Hield, M.J. Brear, S.H. Jin, Thermoacoustic limit cycles in a premixed laboratory combustor with open and choked exits, *Combustion and Flame* 156 (2009) 1683–1697.
[44] M.A. Macquisten, A.P. Dowling, Low-frequency combustion oscillations in a model afterburner, *Combustion and Flame* 94 (1994) 253–264.
[45] T. Sattelmayer, Influence of the combustor aerodynamics on combustion instabilities from equivalence ratio fluctuations, *Journal of Engineering for Gas Turbines and Power* 125 (2003) 11–19.
[46] A.P. Dowling, S.R. Stow, Acoustic analysis of gas turbine combustors, *Journal of Propulsion and Power* 19 (2003) 751–764.
[47] C.S. Goh, A.S. Morgans, The influence of entropy waves on the thermoacoustic stability of a model combustor, *Combustion Science and Technology* 185 (2013) 249–268.
[48] E. Motheau, L. Selle, Y. Méry, T. Poinsot, F. Nicoud, A mixed acoustic-entropy combustion instability in a realistic gas turbine, *Proceedings of the 2012 Summer Program*, Center for Turbulence Research, NASA AMES, Stanford University, USA, pp. 449–458.
[49] E. Motheau, Y. Méry, F. Nicoud, T. Poinsot, Analysis and modeling of entropy modes in a realistic aeronautical gas turbine, *Journal of Engineering for Gas Turbines and Power* 135 (2013) 092602.